

Geometric dynamical observables in rare gas crystals

Lapo Casetti*

Scuola Normale Superiore, Piazza dei Cavalieri 7, 56126 Pisa, Italy

Alessandro Macchi[†]

Istituto Nazionale di Fisica della Materia (INFM), Unità di Firenze, Largo E. Fermi 2, 50125

Firenze, Italy

(Novembre 20, 1996)

Abstract

We present a detailed description of how a differential geometric approach to Hamiltonian dynamics can be used for determining the existence of a crossover between different dynamical regimes in a realistic system, a model of a rare gas solid. Such a geometric approach allows to locate the energy threshold between weakly and strongly chaotic regimes, and to estimate the largest Lyapunov exponent. We show how standard methods of classical statistical mechanics, i.e. Monte Carlo simulations, can be used for our computational purposes. Finally we consider a Lennard Jones crystal modeling solid Xenon. The value of the energy threshold turns out to be in excellent agreement with the numerical estimate based on the crossover between slow and fast relaxation to equilibrium obtained in a previous work by molecular dynamics simulations.

PACS number(s): 05.45.+b, 02.40.-k, 05.20.-y

Typeset using REVTeX

I. INTRODUCTION

Generic non-integrable Hamiltonian systems with $N \geq 3$ degrees of freedom always have a connected chaotic component in phase space. Moreover, as N is large, the measure of such a component should be practically coincident with the measure of the whole constant-energy hyper-surface. In fact, as discussed in Refs. [1–3], the invariant tori whose existence is predicted by the Kol'mogorov-Arnol'd-Moser (KAM) theorem have a positive measure only below a critical value for the amplitude of the non-integrable part of the Hamiltonian, and this critical amplitude is estimated to be rapidly decreasing with N . This does not mean that particular cases in which the KAM threshold is relevant also in macroscopic systems cannot exist, nevertheless it suggests that such a situation could be hardly generic.

These facts support the expectation that varying the energy – or more precisely the energy density $e = E/N$ which is the physical parameter as N is large and eventually as the limit $N \rightarrow \infty$ is taken – one should not observe any qualitative change in the dynamical behavior of large non-integrable Hamiltonian systems. The dynamics should be completely chaotic at all energies, and the only effect of a variation of the energy should be a somewhat trivial rescaling of the characteristic instability time scale, measured by the inverse of the Lyapunov exponent λ . An example of this kind of behavior is provided by self-gravitating systems [4].

On the contrary, there is now a widely accepted numerical evidence that – at least as long as models of nonlinear coupled oscillators are considered – there exist qualitatively different regimes in the dynamics, which have been referred to as weak and strong chaos [1,2]. In the strongly chaotic regime which corresponds to the above sketched scenario, fast phase-space mixing is observed regardless of the initial conditions. At variance, in correspondence of weak chaos one can observe very long mixing times with non-equilibrium initial conditions, and the details of the dynamics are strongly influenced by the choice of the initial conditions. Moreover, at least on finite time scales, the dynamics appears as globally recurrent, as is probed by the probability distribution of single-particle autocorrelation functions [5]. This

effect was observed in several numerical simulations [6,7] inspired by the results of the celebrated numerical experiment by Fermi, Pasta and Ulam (FPU) [8] where the expected equipartition of energy among normal modes was not observed in a chain of linear oscillators coupled by a weak anharmonicity.

The transition between weak and strong chaos is rather sharp when detected looking at non-equilibrium properties, i.e. observing the time behavior of observables which depend on the choice of a particular dynamical initial condition in which the system is far from thermodynamic equilibrium. Examples of these observables are the relaxation times of several dynamical observables to their equilibrium value [1,2], the finite-time values of the so-called spectral entropy [7,9], and the already mentioned probability distributions of single-particle autocorrelation functions [5]. The behavior of these observables neatly detects a threshold value $e = e_c$ which marks the transition between weak and strong chaos, and has been referred to as the strong stochasticity threshold (SST) [1–4,10], or as the crossover energy (CE) [11]. All these observables have the drawback of being not globally defined, i.e. of depending on a particular choice of the initial condition, which could in principle depend on N .

It is remarkable that also the Lyapunov exponent λ , an observable which is neither dependent on the initial conditions nor on N , and which measures directly the degree of chaos, marks the SST. In fact in correspondence of e_c the dependence of λ on e has a crossover: in the strongly chaotic regime one finds a power law which can be successfully predicted by a random matrix approximation (RMA) for the tangent dynamics [2]. In this regime the RMA yields good predictions also for the shape of the whole spectrum of Lyapunov exponents [12]. At variance, in the weakly chaotic case λ is still positive – for nonlinear coupled oscillators $\lambda \propto e^2$ – thus indicating that chaos is present, but the RMA is no longer able to predict its dependence on e . The breakdown of the RMA is a clue that some global change has happened in the phase space structure. The drawback of using the dependence of λ on the energy density as a probe of the SST is that the transition is no longer sharp as in the case of non-equilibrium observables: at e_c , $\lambda(e)$ exhibits only a

crossover between different asymptotic behaviors.

The deep origin of these puzzling dynamical features of non-integrable Hamiltonian systems with many degrees of freedom has at present not yet been understood: nevertheless, a recently proposed differential geometrical approach to Hamiltonian chaos [3] has established a link between the SST and some major change of the geometric structure underlying the dynamics, allowing an operative definition of this threshold no longer based on the computation of time-asymptotic quantities like Lyapunov exponents, but on statistical averages of geometric observables. Starting from the results of Ref. [3] it has been proved the stability of the SST in the thermodynamic limit $N \rightarrow \infty$, at least for the one-dimensional FPU model [10]. Moreover this approach provides the basic tools to obtain a model scalar equation which describes the main features of chaos being independent of the details of the dynamics [13]. The present work follows this geometric approach.

It is worth mentioning that very recently another kind of geometric approach has been put forward [14] which is based on the geometric properties of the trajectories – seen as curves in \mathbb{R}^{2N} – rather than on the properties of the ambient manifolds. As long as a comparison is possible, the two approaches yield perfectly consistent results.

The phenomenology related to the SST has been mainly studied in connection with one-dimensional models of coupled oscillators (FPU model and lattice φ^4 classical model [1–3]), and some numerical results for two-dimensional crystals [15] strongly suggest that a transition between weak and strong chaos is present in more realistic systems. The present work is concerned with the possibility of the existence of the SST in a realistic system, in the perspective of a possible experimental verification of the physical consequences of the transition between weak and strong chaos. Such an experiment has been recently proposed [11], and should verify the existence of a crossover between slow and fast relaxation to thermal equilibrium in a rare gas crystal with diluted impurities. The far-from-equilibrium dynamics of such a system has been studied numerically in Ref. [11], showing that the crossover occurs at $e \simeq 0.15\varepsilon$, where ε is the depth of the interaction potential well. The present work is concerned with the equilibrium dynamical properties of a simpler but closely

related system, i.e. a model of a rare gas solid without impurities. As discussed in Ref. [11], the role played by impurities is crucial to obtain suitable initial conditions in the non-equilibrium case, but should have only a weak effect on the global dynamical properties of the system (this fact is confirmed in a 1-d case [16]), hence the eventual existence of a SST in our model system – apart from being interesting by itself – could have a significance in explaining the phenomenology observed in Ref. [11].

More precisely, the model studied in the present work is a system of n point masses arranged on a three-dimensional fcc lattice with nearest-neighbor Lennard-Jones interaction. The classical dynamics of such a system is a reasonable approximation of the behavior of a rare gas crystal if quantum effects can be neglected, i.e. as long as the temperature is high enough. Hence the existence of a crossover between weak and strong chaos in this model could have a substantial physical relevance if it occurs at e values allowing a classical description of the dynamics, at least as a first approximation. As we shall see in Sec. IV, this happens at least in the case of Xe crystals.

The present work is organized as follows: in Sec. II the geometrical methods which allow a characterization of the transition between weak and strong chaos are sketched; these methods were introduced in Refs. [3,10] and [13], where all details can be found. The model studied is described in Sec. III, and the results are presented and discussed in Sec. IV. Some conclusions are drawn in Sec. V.

II. RIEMANNIAN GEOMETRY AND CHAOTIC DYNAMICS

Hamiltonian dynamics can be rephrased in geometrical terms owing to the fact that the trajectories of a dynamical system with quadratic kinetic energy can be seen as geodesics of a suitable Riemannian manifold. There are several choices for the ambient manifold as well as for the metric tensor. As already discussed in Ref. [10] a particularly useful ambient space is the enlarged configuration space-time $M \times \mathbb{R}^2$, i.e. the configuration space $\{q^1, \dots, q^i, \dots, q^N\}$ with two additional real coordinates q^0 and q^{N+1} . In the following q^0 will

be identified with the time t . For standard Hamiltonians $\mathcal{H} = T + V(\mathbf{q})$ where $T = \frac{1}{2}a_{ij}\dot{q}^i\dot{q}^j$, this manifold, equipped with Eisenhart's metric g_E , has a semi-Riemannian (Lorentzian) structure ($\det g_E = -1$). The arc-length is given by

$$ds^2 = a_{ij}dq^i dq^j - 2V(\mathbf{q})(dq^0)^2 + 2dq^0 dq^{N+1} , \quad (1)$$

where both i and j run between 1 and N . Let us restrict to geodesics whose arc-length parametrization is affine, i.e. $ds^2 = 2C_1^2 dt^2$; simple algebra shows that the geodesic equations

$$\frac{d^2 q^\mu}{ds^2} + \Gamma_{\nu\lambda}^\mu \frac{dq^\nu}{ds} \frac{dq^\lambda}{ds} = 0 \quad \mu, \nu, \lambda = 0 \dots N + 1 , \quad (2)$$

become Newton equations (without loss of generality $a_{ij} = \delta_{ij}$ is considered)

$$\frac{d^2 q^i}{dt^2} = -\frac{\partial V}{\partial q_i} \quad (3)$$

for $i = 1 \dots N$, together with two extra equations for q^0 and q^{N+1} which can be integrated to yield

$$q^0 = t \quad (4a)$$

$$q^{N+1} = C_1^2 t + C_2 - \int_0^t L(\mathbf{q}, \dot{\mathbf{q}}) dt \quad (4b)$$

where $L(\mathbf{q}, \dot{\mathbf{q}})$ is the Lagrangian, and C_1, C_2 are real constants. As stated by Eisenhart theorem [17], the dynamical trajectories in configuration space are projections on M of the geodesics of $(M \times \mathbb{R}^2, g_E)$.

In the geometrical framework, the stability of the trajectories is mapped on the stability of the geodesics, hence it can be studied by the Jacobi equation for geodesic deviation

$$\frac{D^2 J}{ds^2} + R(\dot{\gamma}, J)\dot{\gamma} = 0 , \quad (5)$$

where R is the Riemann curvature tensor, $\dot{\gamma}$ is the velocity vector along the reference geodesic $\gamma(s)$, D/ds is the covariant derivative and J , which measures the deviation between nearby geodesics, is referred to as the Jacobi field. The stability – or instability – of the dynamics, and thus deterministic chaos, originates from the curvature properties of the ambient manifold. In local coordinates, Eq. 5 is written as

$$\frac{D^2 J^\mu}{ds^2} + R_{\nu\rho\sigma}^\mu \frac{dq^\nu}{ds} J^\rho \frac{dq^\sigma}{ds} = 0 , \quad (6)$$

and as already shown in Refs. [3,10], in the case of Eisenhart metric it simplifies to

$$\frac{d^2 J^i}{dt^2} + \frac{\partial^2 V}{\partial q_i \partial q^j} J^j = 0 , \quad (7)$$

which is nothing but the usual tangent dynamics equation for standard Hamiltonians. The Lyapunov exponents are usually computed evaluating the rate of exponential growth of J by means of a numerical integration of Eq. (7) [18].

In the particular case of *constant curvature* manifolds, Eq. (5) becomes very simple [19]

$$\frac{D^2 J^\mu}{ds^2} + K J^\mu = 0 , \quad (8)$$

and has bounded oscillating solutions $J \approx \cos(\sqrt{K} s)$ or exponentially unstable solutions $J \approx \exp(\sqrt{-K} s)$ according to the sign of the constant sectional curvature K , which is given by

$$K = \frac{K_R}{N-1} = \frac{\mathcal{R}}{N(N-1)} , \quad (9)$$

where $K_R = R_{\mu\nu} \dot{q}^\mu \dot{q}^\nu$ is the Ricci curvature and $\mathcal{R} = R^\mu_\mu$ is the scalar curvature; $R_{\mu\nu}$ is the Ricci tensor. Manifolds with $K < 0$ are considered in abstract ergodic theory (see e.g. Ref. [20]). Krylov [21] originally proposed that the presence of some negative curvature could be the mechanism actually at work to make chaos in physical systems, but in realistic cases the curvatures are neither found constant nor everywhere negative, and the straightforward approach based on Eq. (8) does not apply. This is the main reason why Krylov's ideas remained confined to abstract ergodic theory with few exceptions.

In spite of these major problems, some approximations on Eq. (5) are possible even in the general case. The key point is that negative curvatures are not strictly necessary to make chaos, and that a subtler mechanism related to the *bumpiness* of the ambient manifold is actually at work.

Let us choose a geodesic frame (i.e. a reference frame which is parallel transported along a geodesic; as a consequence, $D/ds \equiv d/ds$), and project Eq. (5) on a direction determined by the unit vector u :

$$\frac{d^2}{ds^2} \langle J, u \rangle + \langle R(\dot{\gamma}, J)\dot{\gamma}, u \rangle = 0 . \quad (10)$$

If the system is chaotic, J grows exponentially with growth rates given by the Lyapunov exponents, and if u is the direction corresponding to the largest Lyapunov exponent λ , after a finite (proper) time s the components of J along the other directions will become negligible compared to that along u , thus we find $J \approx \psi u$. Equation (10) is thus rewritten approximately as a scalar Hill equation for ψ ,

$$\frac{d^2\psi}{ds^2} + K(s)\psi = 0 , \quad (11)$$

where $K(s) = K(\dot{\gamma}, u)$ is the sectional curvature of the geodesic plane spanned by the directions $\dot{\gamma}$ and u and is no longer a constant, but a fluctuating function taking mostly *positive* values (in some cases like the FPU model K is strictly positive) whence the solutions of Eq. (11) can be subject to *parametric instability*. Curvature fluctuations can produce chaos even if no negative curvature is experienced by the geodesics. As the sectional curvature is no longer constant, K_R and \mathcal{R} are respectively averages of K over the direction of J and over both the direction of J and the direction of the reference geodesic in the latter. Equation (9) no longer holds, nevertheless it is a first order approximation to which an estimate of the curvature fluctuations can be added to obtain a stochastic model of $K(s)$ independent of the dynamics of the system [13]. This model leads to an analytical estimate of the Lyapunov exponent λ , which is correct (at least for the FPU model) in the limit $N \rightarrow \infty$.

Up to this point the results are independent of the choice of the metric. Specializing to the Eisenhart arc-length parametrization Eq. (11) is rewritten in terms of the time t ,

$$\ddot{\psi} + K(t)\psi = 0 , \quad (12)$$

where a dot stands for a time derivative and $K(t) = K(s\sqrt{2C_1^2})/2C_1^2$. The stochastic model of $K(t)$ is given by

$$K(t) = \langle k_R \rangle + \langle \delta^2 k_R \rangle^{1/2} \eta(t) , \quad (13)$$

where $k_R = K_R/N$, $\langle \cdot \rangle$ stands for an average taken along a geodesic, which, for systems in thermal equilibrium, can be substituted with a statistical average taken with respect to a suitable probability measure (e.g. the micro-canonical or the canonical measure); $\eta(t)$ is a stationary δ -correlated Gaussian stochastic process with zero mean and variance equal to one. Using Eisenhart metric, and for standard Hamiltonians, the non-vanishing components of the Riemann tensor are $R_{0i0j} = \partial_{q_i} \partial_{q_j} V$, hence the Ricci curvature has the remarkably simple form

$$k_R = \frac{1}{N} \nabla^2 V , \quad (14)$$

where ∇^2 is the Euclidean Laplacian operator. Equation (12) becomes a stochastic differential equation, i.e. the evolution equation of a random oscillator [22]. It is worth noticing that Eq. (12) is no longer dependent on the dynamics, since the random process depends only on statistical averages. The estimate of the Lyapunov exponent λ is then obtained through the evolution of the second moments of the solution of (12) as

$$\lambda = \lim_{t \rightarrow \infty} \frac{1}{2} \log \frac{\psi^2(t) + \dot{\psi}^2(t)}{\psi^2(0) + \dot{\psi}^2(0)} . \quad (15)$$

As shown in Ref. [13], this yields the following expression for λ :

$$\lambda(k, \delta_k, \tau) = \frac{1}{2} \left(\Lambda - \frac{4k}{3\Lambda} \right) , \quad (16)$$

where

$$\Lambda = \left(\delta_k^2 \tau + \sqrt{\frac{64k^3}{27} + \delta_k^4 \tau^2} \right)^{1/3} , \quad (17a)$$

$$\tau = \frac{\pi \sqrt{k}}{2\sqrt{k(k + \delta_k)} + \pi \delta_k} ; \quad (17b)$$

in the above expressions k is the average Ricci curvature $k = \langle k_R \rangle$ and δ_k stands for the mean-square fluctuation of the Ricci curvature, $\delta_k = \langle \delta^2 k_R \rangle^{1/2}$.

The advantages in using the geometric approach to Hamiltonian chaos are thus evident. In fact, it is possible to give reliable estimates of the Lyapunov exponent without actually

computing the time evolution of the system: the estimate (16) of λ depends only on statistical averages which can be either computed analytically in some cases (for instance in the case of the FPU model [13]) or, in general, extracted from a Monte Carlo simulation, as it is the case of the model to be studied in the present work.

The behavior of the average geometric observables as the control parameter (e.g. the energy density or the temperature) is varied conveys an information which goes beyond the possibility of computing the Lyapunov exponent. The dependence of the average Ricci curvature on the energy density has already been used in Ref. [10] to give an operational definition of the SST which allows its computation in the thermodynamic limit, showing the stability of the threshold in this limit for the FPU model. In fact, it is easy to find that for a harmonic chain $\langle k_R \rangle$ is constant as the energy density is varied, and this is a common feature of other integrable models (e. g. the Toda chain [10]). A computation of $\langle k_R \rangle(e)$ at constant volume (length) for the FPU chain shows that the average Ricci curvature exhibits two well-defined asymptotic behaviors, $\langle k_R \rangle(e) = \text{const.}$ as $e \rightarrow 0$ (harmonic limit), and $\langle k_R \rangle(e) = e^{1/2}$ as $e \rightarrow \infty$. The crossover between the two asymptotic curves occurs at a value of e , e_c , which can be interpreted as a geometric estimate of the SST. Such a geometric estimate is in very good agreement with estimates based on other methods.

Moreover, one can look at the random oscillator equation (12) as an effective Jacobi equation for a geodesic flow on a surface M whose Gaussian curvature is given by the random process $K(t)$. As long as nonlinear coupled oscillators are considered, the average Ricci curvature is positive, hence M can be regarded as a sphere with a fluctuating radius. In the limit of vanishing fluctuations, one recovers the bounded evolution of the Jacobi field associated with integrable dynamics. Chaos suddenly appears as curvature fluctuations are turned on, nevertheless it will be “weak” as long as $\delta_k \ll k$, i.e. as long as M can be considered as a weakly perturbed sphere. On the contrary as the size of curvature fluctuations becomes of the same order of the average curvature, $\delta_k \approx k$, M can no longer resemble a sphere, and the dynamics will no longer “feel” the integrable limit. Hence we expect the dynamics to be strongly chaotic. This is by no means a deep explanation of the

existence of weakly and strongly chaotic regimes in Hamiltonian dynamics. Nevertheless it shows how the simple geometric concepts which enter the Riemannian description of Hamiltonian chaos, besides providing effective computational tools, are also useful in helping one's physical intuition with images and analogies which would be difficult to find elsewhere.

III. THE MODEL AND THE GEOMETRIC OBSERVABLES

The system studied in the present work is a crystal of n atoms of mass m moving in three dimensions and interacting through a pairwise central potential $v(r)$. Its Hamiltonian is

$$\mathcal{H} = \frac{1}{2m} \sum_{i=1}^n \mathbf{p}_i^2 + V(\mathbf{X}) \quad (18)$$

where

$$V(\mathbf{X}) = \frac{1}{2} \sum_{i,j=1}^n v(|\mathbf{x}_i - \mathbf{x}_j|) , \quad (19)$$

The geometric observables which, within the approximations described in the previous Section, are relevant to the dynamical instability of the system, are the average Ricci curvature of $(M \times \mathbb{R}^2, g_E)$ and its fluctuations. In the case of a pairwise interaction potential the Ricci curvature turns out to be (see Eq. 14):

$$k_R = \frac{1}{N} \sum_{i=1}^n \sum_{j_i=1}^{12} v''(|\mathbf{x}_i - \mathbf{x}_{j_i}|) + 2 \frac{v'(|\mathbf{x}_i - \mathbf{x}_{j_i}|)}{|\mathbf{x}_i - \mathbf{x}_{j_i}|} , \quad (20)$$

where it should be noticed that $N = 3n$ as it represents the number of degrees of freedom.

The quantities which have to be determined are

$$k = \langle k_R \rangle \quad (21a)$$

$$\delta_k^2 = \langle \delta^2 k_R \rangle = \frac{1}{N} (\langle k_R^2 \rangle - \langle k_R \rangle^2) . \quad (21b)$$

The probability measure which is usually employed for computational purposes is the canonical distribution so that the statistical averages of Eqs.(21) can be written as

$$\langle f \rangle(\beta) = Z_C^{-1} \int d\mathbf{X} f(\mathbf{X}) e^{-\beta V(\mathbf{X})} , \quad (22)$$

where Z_C is the configurational part of the canonical partition function,

$$Z_C = \int d\mathbf{X} e^{-\beta V(\mathbf{X})} . \quad (23)$$

As a matter of fact in the canonical statistical ensemble the role of control parameter is played by the inverse temperature $\beta = 1/k_B T$ where k_B is the Boltzmann's constant. However, in the thermodynamic limit ($N \rightarrow \infty$), the micro-canonical averages can also be obtained from the canonical ones. As long as the mean value $k = \langle k_R \rangle$ is concerned, the canonical and microcanonical averages differ only by a $\mathcal{O}(1/N)$ correction. Hence in the thermodynamic limit

$$\langle k_R \rangle (e) = \langle k_R \rangle (\beta (e)) , \quad (24a)$$

$$e(\beta) = \frac{1}{2\beta} - \frac{1}{N} \frac{\partial}{\partial \beta} [\log Z_C(\beta)] . \quad (24b)$$

As regards $\delta_k^2 = \langle \delta^2 k_R \rangle$, one must keep in mind that fluctuations depend on the statistical ensemble. In fact the difference between canonical and microcanonical fluctuations does not vanish in the thermodynamic limit and the relation between these two quantities is, according to Ref. [23],

$$\langle \delta^2 k_R \rangle (e) = \langle \delta^2 k_R \rangle (\beta (e)) + F(\beta (e)) , \quad (25a)$$

$$F(\beta) = -\frac{k_B \beta^2}{c_v} \left(\frac{\partial \langle k_R \rangle}{\partial \beta} \right)^2 , \quad (25b)$$

where $e(\beta)$ is given again by Eq.(24b) and c_v is the specific heat at constant volume. Thus the micro-canonical fluctuations can be obtained from the canonical ones provided that the values of the specific heat are known.

IV. RESULTS AND DISCUSSION

The geometric observables described in the previous Sections have been evaluated for a Lennard-Jones face-centered cubic (fcc) crystal whose Hamiltonian is given by Eqs.(18) and (19) with a pair interaction potential which reads

$$v(r) = 4\epsilon \left[\left(\frac{\sigma}{r} \right)^{12} - \left(\frac{\sigma}{r} \right)^6 \right] . \quad (26)$$

Through an appropriate choice of the free parameters m (mass), ϵ and σ , this simple model is able to take account of most thermodynamical properties of rare gas solids.

The statistical averages of Eqs. (21) have been calculated by means of a standard canonical Monte Carlo algorithm where a simulation box of $n = 256$ particles subjected to periodic boundary conditions has been used. In all simulations only nearest neighbors interactions have been dynamically taken into account; the contributions of the interactions beyond the nearest neighbors shell has been considered in a “static approximation” in which the instantaneous relative positions of the atoms are replaced by their equilibrium values. Apparently this procedure does not affect the evaluation of the geometrical observables; its advantage resides in the fact that allows one to employ the all neighbors parameters ϵ and σ which give a reasonable representation of the real pair potential and the equation of state of rare gas solids [25].

All data reported here are given in dimensionless form by reducing them with respect to the “natural units” of the model; namely the reduced energy is measured in unit of ϵ and the Ricci curvature in unit of ϵ/σ^2 as well as its mean-square fluctuation.

We performed two distinct series of simulations. In the first series the density ρ of the crystal has been kept constant in order to compare the qualitative behaviour of the geometric observables with the known results for one-dimensional systems. In fact, computations of chains of anharmonic oscillators have been performed at constant length [3,10,16]. The numerical outcomes of this series of simulations are reported in Figs. 1-3 where k , δ_k/k and the estimate λ of the Lyapunov exponent computed according to Eq. (16) are plotted

versus the energy per degree of freedom of the system. The additional data appearing in these figures refer to computations where the interaction potential (26) has been expanded up to the fourth order in the Taylor series. This procedure allows us to perform simulations at higher energies in order to provide a better representation of the crossover energy region. The results reported in Fig. 1 show that the SST, or crossover energy, can be located around $e_c \simeq 0.15$. This estimate of e_c is confirmed by the results reported in Fig. 2, for Fig. 2 shows that in correspondence of this threshold the ratio δ_k/k deviates remarkably from the low-energy behaviour $\delta_k/k \propto e$ and tends to saturate towards $\delta_k/k \simeq 1$ which implies that the manifold becomes highly anisotropic, and thus we expect the dynamics to enter the strongly chaotic regime. As a consequence of the behaviour of k and δ_k , the geometric estimate λ of the Lyapunov exponent shows a sharp crossover between two different power laws. It is worth recalling that the quantity here reported is not the “true” Lyapunov exponent but an estimate which has anyhow proven to be extremely accurate in other systems [13].

The aim of the second series of simulations is mainly to determine whether the averages of the geometric observables are affected by a change in the density of the sample. In principle one expects such a change because the curvature properties depend on space derivatives, and a change of the density induces a change in the length scale. Moreover, it is interesting to test the expectation that the crossover in the relaxation behaviour of a Xe crystal recently observed in numerical simulations [11], is related with some major change in the global properties of the dynamics (i.e. the SST) which in turn can be detected by the geometric observables under investigation in this paper. Hence it is interesting to compute the statistical averages of Eqs. (21) using settings which are close to those used in the molecular dynamics simulations reported in [11]. In particular the results shown in Figs. 3-6 refer to the values of the density given by the empirical equation of state of solid Xe ($\varepsilon/k_B = 228.6^\circ \text{ K}$, $\sigma = 3.959 \text{ \AA}$) [25].

The results reported in Figs. 3-6 show that the qualitative behaviour of the curvature fluctuations (Fig. 5) and of the theoretical estimate of the Lyapunov exponent λ (Fig. 6) is the same as in the constant density case, while the behaviour of the average curvature (Fig.

4) is dramatically altered: instead of a crossover between two asymptotic regimes we have here a neat maximum of k at $e = e_c$. It is remarkable that the value of e_c – as estimated through the behaviour of δ_k or λ or by the position of the maximum of k – remains the same as in the constant density case, and corresponds to a temperature $T \simeq 0.15\varepsilon/k_B$, i.e. occurs at a temperature of physical relevance for the thermodynamics of this system. Moreover, the value of e_c is in excellent agreement with the value of the crossover energy estimated via the nonequilibrium dynamics [11].

Let us now briefly comment about the problem of the relevance of quantum effects for the results presented in this Section. As already stated in the Introduction, our analysis is a completely classical one so that the significance of our results depends on the reliability of the classical approximation of the dynamics in the range of temperatures investigated. The strength of the quantum behavior of the interaction is ruled by a coupling parameter $g = \hbar\omega_{LJ}/\varepsilon$ that is the ratio between the typical vibrational quantum energy $\hbar\omega_{LJ}$ calculated in the harmonic approximation and the binding energy ε . Values $g \ll 1$ denote that quantum effects may be neglected in a wide range of temperatures. However, as observed in Ref. [26], the failure of the classical approximation becomes quite evident for all rare gas solids at measurable temperatures. The detailed evaluation of the influence of quantum effects for the determination of the threshold energy e_c is out of the purposes of this paper. We present here results for solid Xenon where, due to the small coupling parameter ($g = 0.106$), the relevance of quantum effects in our discussion, if any, is certainly not decisive.

V. CONCLUSIONS

We have presented here a detailed description of how a differential geometric approach to Hamiltonian chaos can be used for determining the existence of the SST in a realistic system. We have discussed the connection between the SST and the geometrical observables which have been investigated in this paper. We have shown how standard methods of classical statistical mechanics can be used for our computational purposes. We have finally

applied the framework here developed to a Lennard Jones crystal modeling solid Xenon. The crossover energy region of this system has been clearly detected and the value of the energy threshold has turned out to be in excellent agreement with the numerical results presented in a recent paper [11]. The possibility of setting up an experiment of this system for determining the physical consequences of the transition from weak and strong chaos regime is under investigation.

ACKNOWLEDGMENTS

It is a pleasure to thank Roberto Livi and Marco Pettini for enlightening discussions and for their interest in our work.

REFERENCES

* Also at INFN, sezione di Firenze, Italy. Electronic address: casetti@sns.it.

† Electronic address: macchi@fi.infn.it.

- [1] M. Pettini and M. Landolfi, Phys. Rev. A **41**, 768 (1990).
- [2] M. Pettini and M. Cerruti-Sola, Phys. Rev. A **44**, 975 (1991).
- [3] M. Pettini, Phys. Rev. E **47**, 828 (1993).
- [4] M. Cerruti-Sola and M. Pettini, Phys. Rev. E **51**, 53 (1995).
- [5] S. Isola, R. Livi, and S. Ruffo, Europhys. Lett. **3**, 407 (1987).
- [6] P. Bocchieri, A. Scotti, B. Bearzi, and A. Loinger, Phys. Rev. A **2**, 2013 (1970).
- [7] R. Livi, M. Pettini, M. Sparpaglione, S. Ruffo, and A. Vulpiani, Phys. Rev. A **31**, 1039 (1985); R. Livi, M. Pettini, S. Ruffo, and A. Vulpiani, *ibid.* **31**, 2740 (1985).
- [8] E. Fermi, J. Pasta, and S. Ulam, Los Alamos Report LA-1940, reprinted in *Collected Papers of Enrico Fermi*, edited by E. Segré (University of Chicago, Chicago, 1965), Vol. 2, p. 978.
- [9] H. Kantz, R. Livi, and S. Ruffo, J. Stat. Phys. **76**, 627 (1994).
- [10] L. Casetti and M. Pettini, Phys. Rev. E **48**, 4320 (1993).
- [11] L. Casetti, R. Livi, A. Macchi, and M. Pettini, Europhys. Lett. **32**, 549 (1995).
- [12] G. Paladin and A. Vulpiani, J. Phys. A **19**, 1881 (1986); R. Livi, A. Politi, and S. Ruffo, *ibid.* **19**, 2033 (1986); R. Livi, A. Politi, S. Ruffo, and A. Vulpiani, J. Stat. Phys. **46**, 147 (1987); J.-P. Eckmann, C. E. Wayne, *ibid.* **50**, 853 (1988).
- [13] L. Casetti, R. Livi, and M. Pettini, Phys. Rev. Lett. **74**, 375 (1995); L. Casetti, C. Clementi, and M. Pettini, *Riemannian theory of Hamiltonian chaos and Lyapunov exponents*, chao-dyn/9609010, Phys. Rev. E (in press).

- [14] C. Alabiso, N. Besagni, M. Casartelli, and P. Marenzoni, *J. Phys. A* **29**, 3733 (1996).
- [15] G. Benettin and A. Tenenbaum, *Phys. Rev. A* **28**, 3020 (1983).
- [16] L. Casetti, G. Di Tocco, R. Livi, A. Macchi, M. Pettini, and M. Spicci, in preparation.
- [17] L. P. Eisenhart, *Ann. of Math.* **30**, 591 (1929).
- [18] G. Benettin, L. Galgani, and J. M. Strelcyn, *Phys. Rev. A* **14**, 2338 (1976).
- [19] M. P. do Carmo, *Riemannian geometry*, (Birkhäuser, Boston, 1992).
- [20] Ya. G. Sinai, *Dynamical Systems II*, Encyclopaedia of Mathematical Sciences, Vol. 2 (Springer-Verlag, Berlin, 1989).
- [21] N. S. Krylov, *Works on the foundations of statistical physics*, (Princeton University Press, Princeton, 1979).
- [22] N. G. Van Kampen, *Phys. Rep.* **24**, 171 (1976).
- [23] J. L. Lebowitz, J. K. Percus, and L. Verlet, *Phys. Rev.* **153**, 250 (1967).
- [24] M. Neumann, F. Barocchi, and M. Zoppi, *Phys. Rev. A* **36**, 2440 (1987).
- [25] *Rare Gas Solids*, edited by M. L. Klein and J. A. Venables, (Academic, London, 1976)
- [26] A. Cuccoli, A. Macchi, V. Tognetti and R. Vaia, *Phys. Rev. B* **47**,14923 (1993).

FIGURES

FIG. 1. Average Ricci curvature k vs the energy per degree of freedom at constant density ($\rho = 1.0$ in natural units). Open circles: data of computations where the interaction potential (26) has been expanded up to the fourth order in the Taylor series; solid circles: data obtained with the “full” interaction potential (26). The two dotted lines represent the estimated low- and high-energy behaviours of k helping the identification of e_c ; the line interpolating the high-energy data has been obtained by fitting a law $k \approx \alpha + \beta e^{1/2}$, with fitting parameters α and β , to the high-energy data.

FIG. 2. Normalized mean-square fluctuation of the Ricci curvature δ_k/k vs the energy per degree of freedom at constant density. Symbols as in Fig. 1. The dotted line is the linear behaviour.

FIG. 3. Theoretical estimate of the Lyapunov exponent λ according to Eq. (16) versus the energy per degree of freedom at constant density. Symbols as in Fig. 1. The dotted line is the power law e^2 .

FIG. 4. Average Ricci curvature k vs the energy per degree of freedom. Here, in each simulation we have used values of the density according to the empirical equation of state of solid Xenon.

FIG. 5. The same as Fig. 4 for the normalized means-square fluctuation of the Ricci curvature δ_k/k . The dotted line is the linear behaviour.

FIG. 6. The same as Fig. 4 for the estimate of the Lyapunov exponent λ . The dotted line is the law e^2 .

Fig. 1

L. Casetti and A. Macchi "Geometric dynamical..."

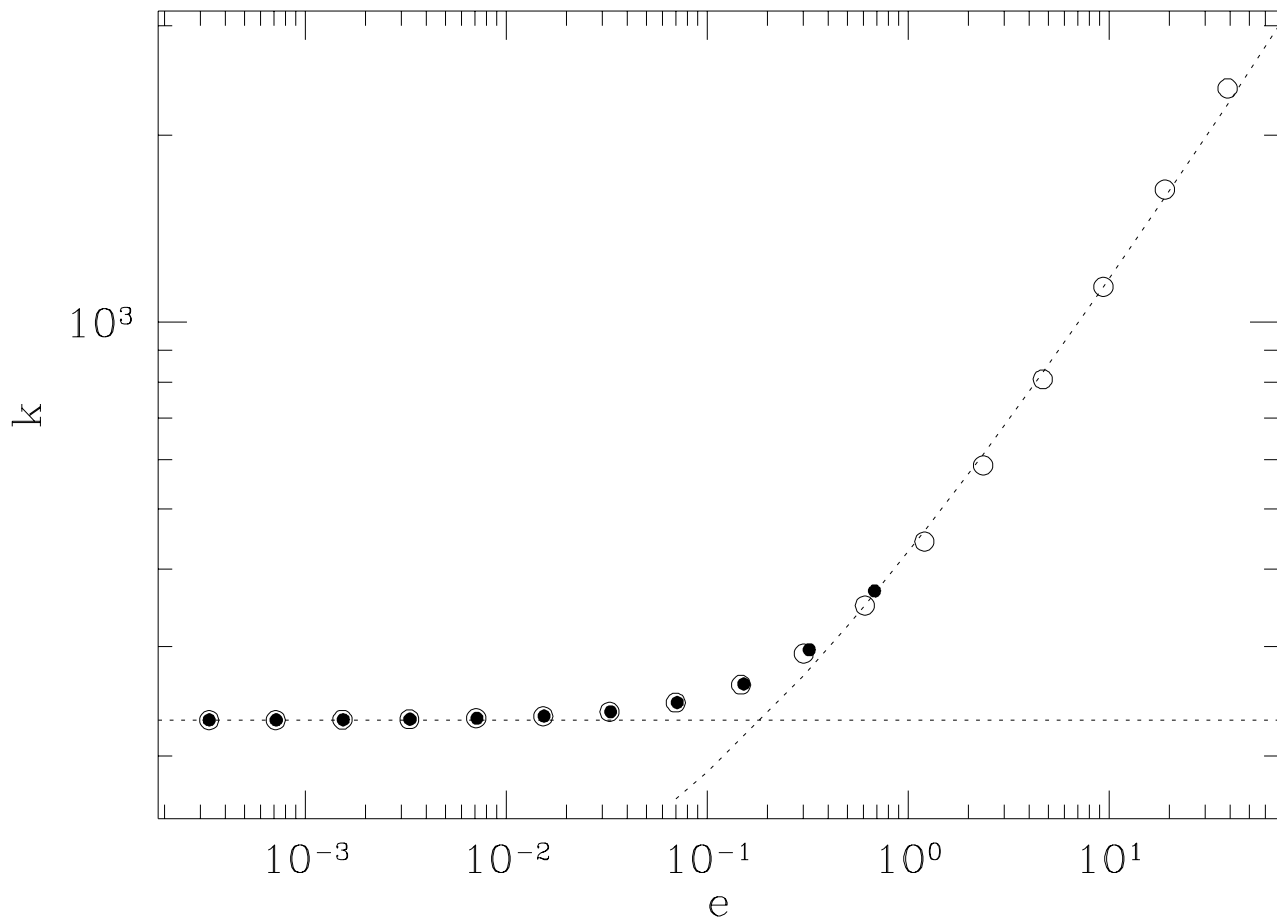


Fig. 2

L. Casetti and A. Macchi “Geometric dynamical...”

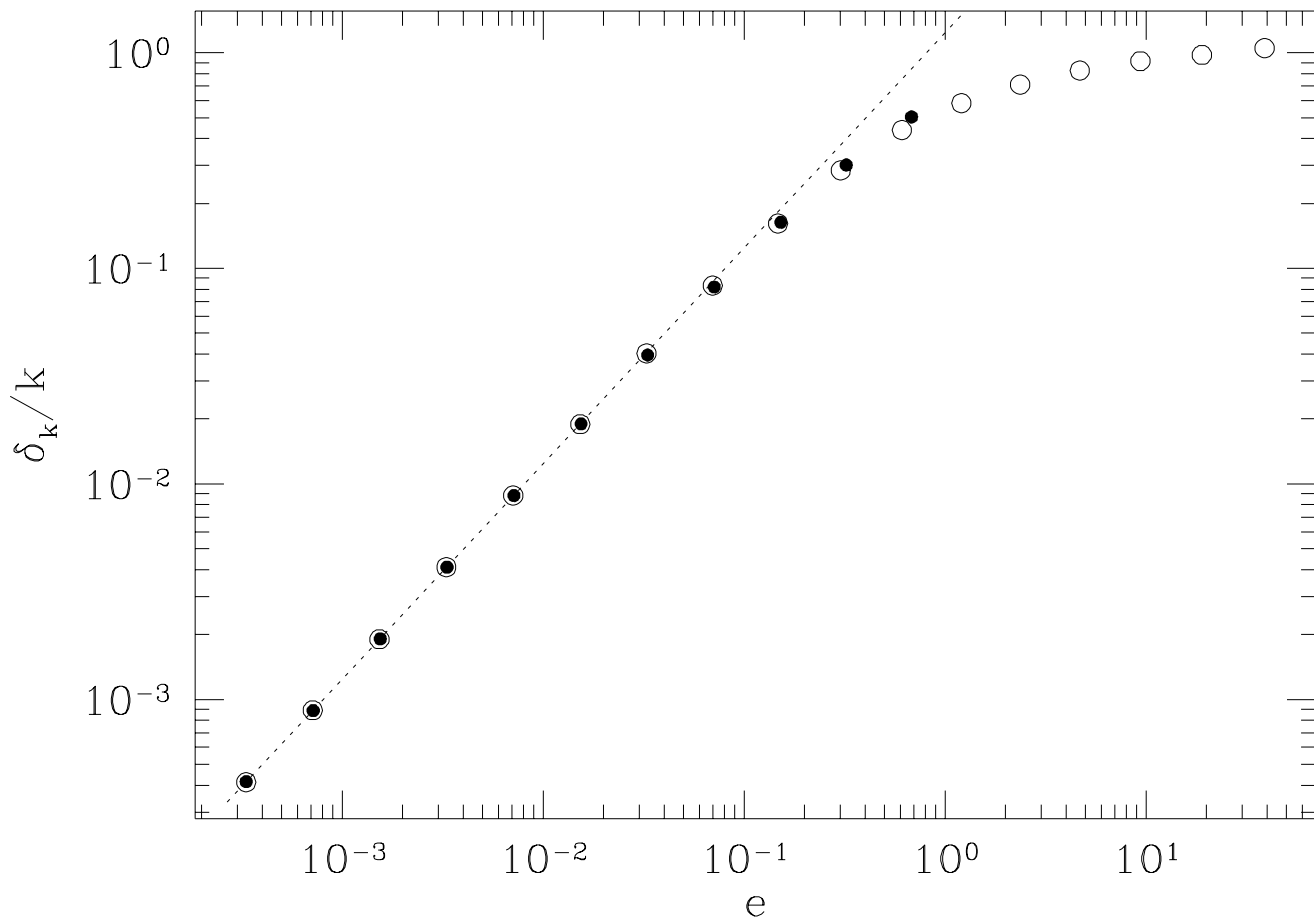


Fig. 3

L. Casetti and A. Macchi “Geometric dynamical...”

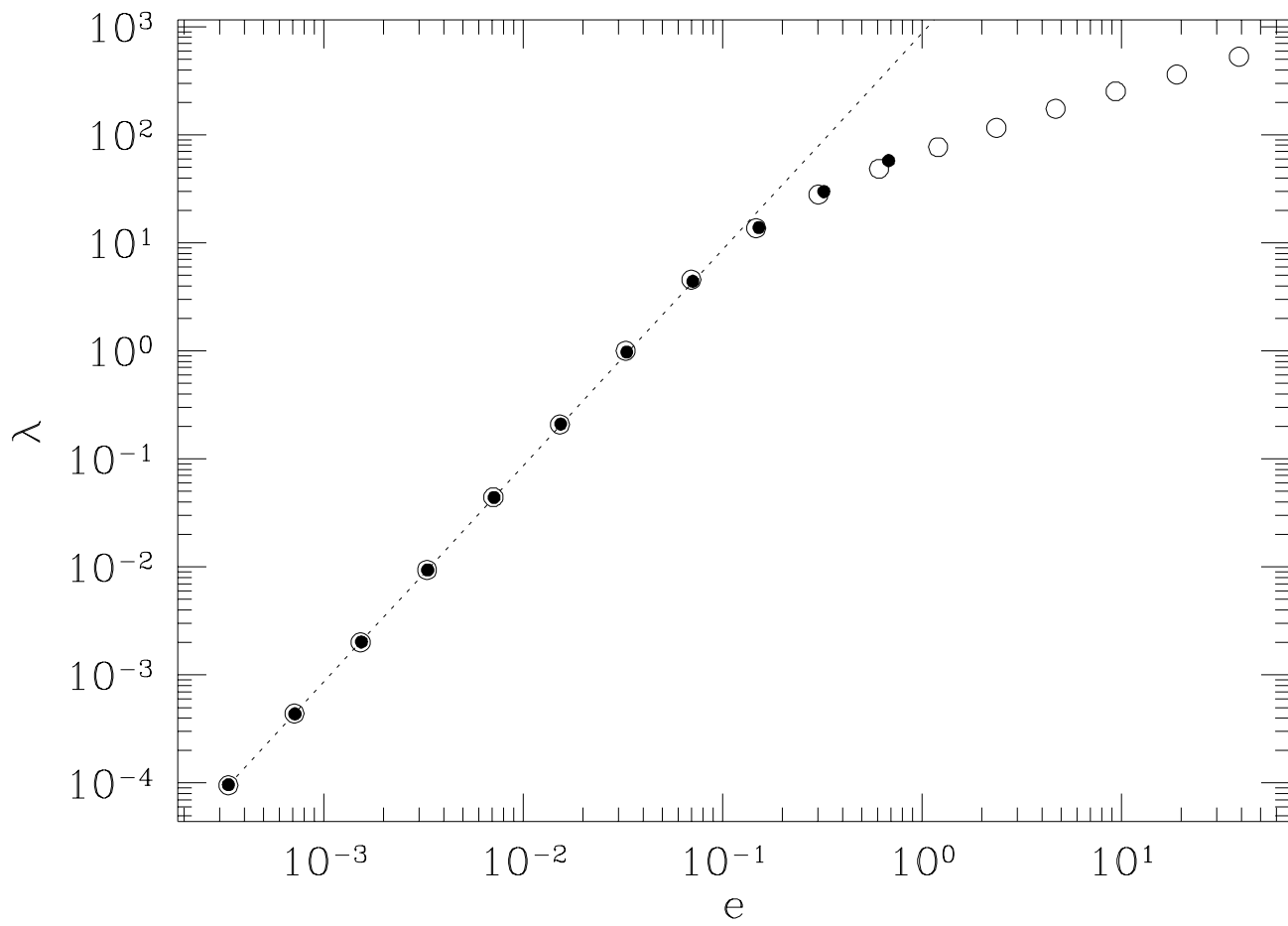


Fig. 4

L. Casetti and A. Macchi “Geometric dynamical...”

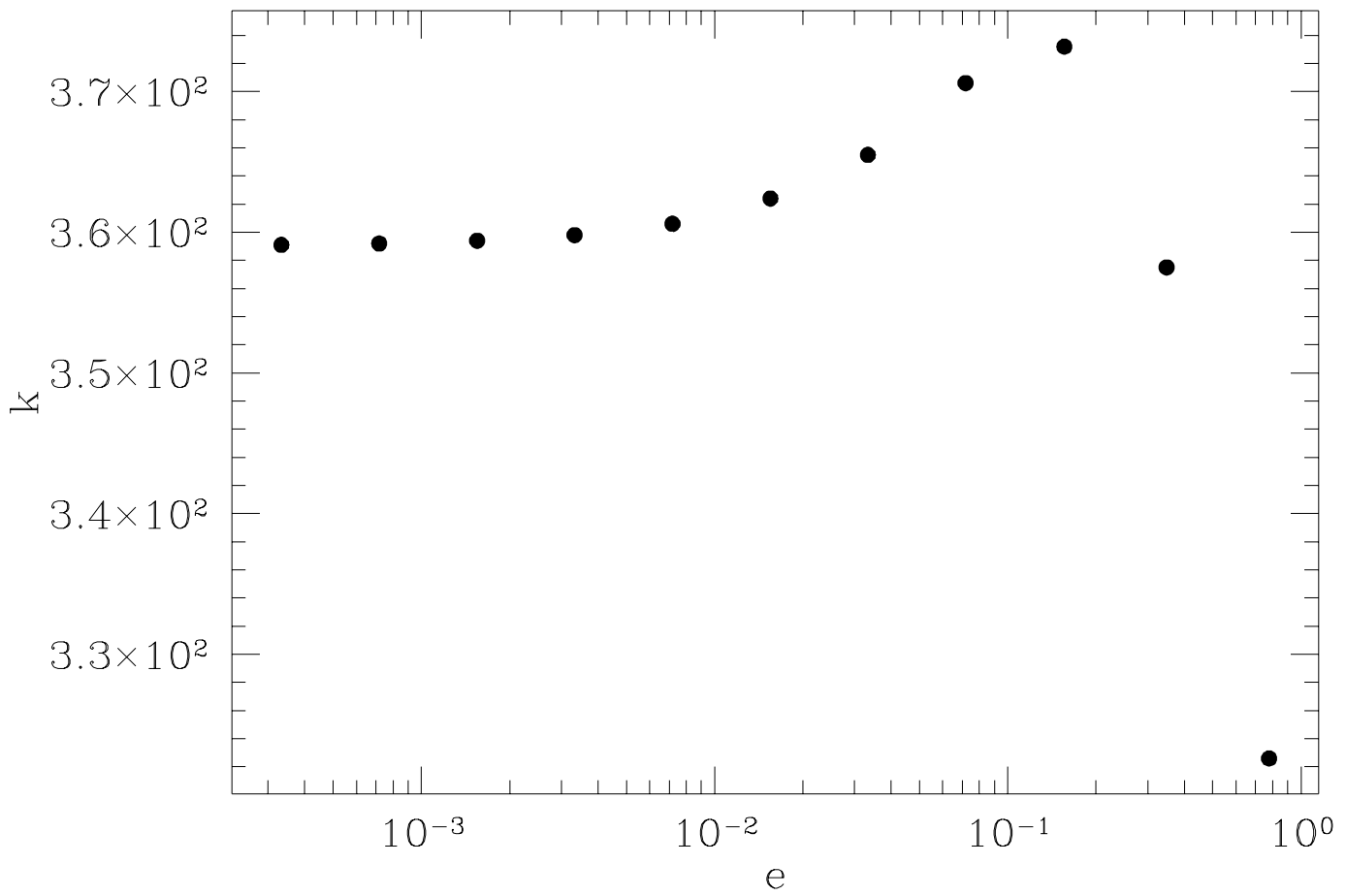


Fig. 5

L. Casetti and A. Macchi “Geometric dynamical...”

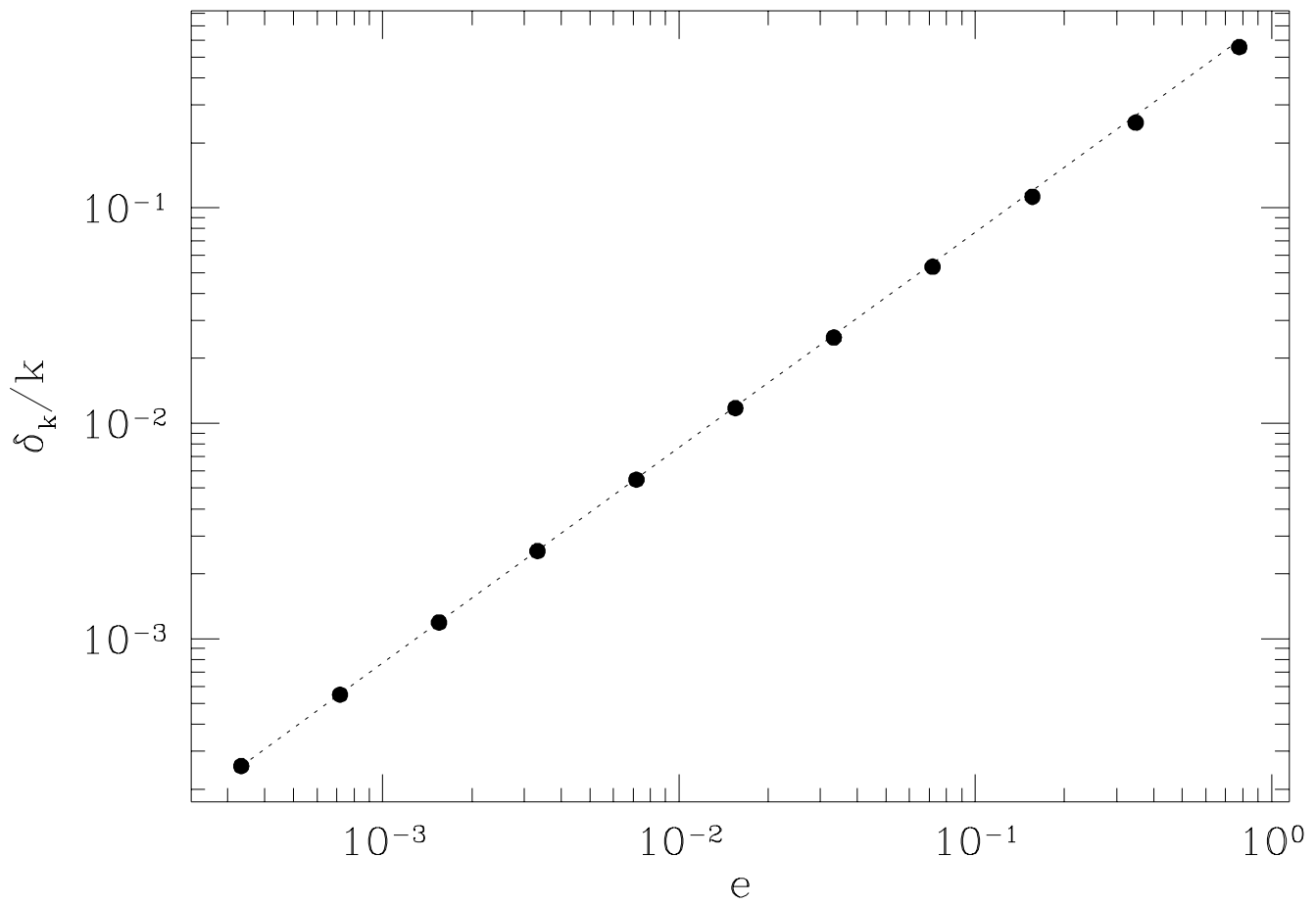


Fig. 6

L. Casetti and A. Macchi “Geometric dynamical...”

